ISSN 0018-151X, High Temperature, 2018, Vol. 56, No. 2, pp. 247–254. © Pleiades Publishing, Ltd., 2018.
Original Russian Text © L.A. Benderskii, D.A. Lyubimov, A.O. Chestnykh, B.M. Shabanov, A.A. Rubakov, 2018, published in Teplofizika Vysokikh Temperatur, 2018, Vol. 56, No. 2, pp. 261–269.

HEAT AND MASS TRANSFER AND PHYSICAL GASDYNAMICS

The Use of the RANS/ILES Method to Study the Influence of Coflow Wind on the Flow in a Hot, Nonisobaric, Supersonic Airdrome Jet during Its Interaction with the Jet Blast Deflector

L. A. Benderskii[a], *, D. A. Lyubimov[a], **, A. O. Chestnykh[a], *, B. M. Shabanov[b], and A. A. Rubakov[b]**

[a]*Central Institute of Aviation Motors, Moscow, Russia*
[b]*Joint Supercomputer Center, Russian Academy of Sciences, Moscow, Russia*
**e-mail: Leosun.ben@gmail.com*
***e-mail: lyubimov@ciam.ru*
****e-mail: a.o.chestnyh@gmail.com*

Received July 12, 2016

Abstract—The influence of the coflow wind on the flow in a hot, nonisobaric, supersonic airdrome jet from a biconical nozzle and its interaction with a jet blast deflector (JBD) are studied by the RANS/ILES method. The conditions at the external boundary of the computational domain are formulated for the problem of jet interaction with the JBD. All calculations were performed at the Joint Supercomputer Center of the Russian Academy of Sciences with a MVS-10P supercomputer. The features of method parallelization for the supercomputer with modern architecture are described. The total temperature of the jet at the nozzle output is $T_0 = 1050$ K and $\pi_c = 4$. The wind velocity ranges from 0 to 20 m/s. Two JBD positions are examined: at distances of 5 and $15D_e$ of the nozzle cross section. The computation grids consist of $(6.33–8.53) \times 10^6$ cells. Fields of the flow parameters and of their turbulent pulsations near the jet are obtained. The dimensions of the "safety zone" for people and machinery is determined by the temperature, pressure pulsations, and velocity near the airdrome surface. The influence of wind velocity on the size and shape of the safety zone are revealed. The distributions of pressure and temperature and their pulsations over JBD altitude are presented as a function of JBD position and wind velocity.

DOI: 10.1134/S0018151X18020037

INTRODUCTION

The problem of jet inflow onto an obstacle is a commonly encountered problem in technical applications, and it is therefore actively studied. In the majority of cases, the interaction between a free jet and a large obstacle placed at an angle with to the jet's axis is considered, making it possible to disregard the edge effects. The problem of turbulent jet spreading along a solid surface and its interaction with obstacles (deflector, JBD), the sizes of which are comparable with the jet cross size, is more complicated. However, it is just such situations that are the closest to the real conditions. It is of interest to investigate the interaction of high-velocity reactive jets from turbojet engines (TJEs) and the JBD. Such problems appear when an aircraft with an operating engine is at the airdrome near the JBD and at liftoff from naval deck aircrafts. In these cases it is necessary to know the safety zone for people and machinery at the airdrome, beyond which the temperature, pressure pulsations and jet velocity are not higher than the predetermined values. For this purpose it is necessary to describe properly the behavior of reactive jets of turbojet aircrafts [1]. This problem is especially relevant for ship's deck aviation, since the deck size is limited, flights are performed under night conditions, and the intensity of aircrafts liftoff is high.

It is necessary to point out that the flow in the circular jet that extends along solid surface develops in a different way than in the free jet: great transversal spreading is seen along the surface [1–5]. The Reynolds averaged Navier–Stokes (RANS) methods with traditional turbulence models do not simulate this process, even qualitatively [6]. In the problem of the interaction of jet exhaust from TJE with the JBD, it is very important to know both the sizes of the safety zones determined according to different parameters and the nonstationary flow characteristics: the pressure and temperature turbulent pulsations on the airdrome surface, on the ship's deck, and on the JBD. It is possible to solve this problem only with the help of vortex-resolvable methods [7], in which turbulent vortexes are resolved explicitly.

It is especially relevant for supersonic jets, since their temperature and pressure are significantly higher than those in subsonic bypass turbojet engines. Expe-

rimental and numerical studies verify this fact. For example, the influence of the temperature of a model supersonic jet, the inclination angle of the JBD, and the distance from it to the nozzle exit on the narrow-band noise in the near and far fields was studied experimentally [8]. The interaction of the nonisobaric supersonic airdrome jet exhaust from the biconical nozzle with the JBD was studied by the MILES method based on Euler equations [9]. The distributions of the flow and turbulence parameters in the jet and on the JBD surface are presented, as well as the acoustic parameters in the near field. In [10], the interaction of a pair of nonisobaric supersonic jets with the JBD was calculated by the LES (large eddy simulation) and RANS/ILES (implicit large eddy simulation) methods. The calculations were performed for a grid consisting of 41×10^6 cells. The numerical and experimental results were in good agreement according to integral noise and for one-third of the octave-band spectrum. The results of numerical studies performed by the LES method are presented in [11] for hot jet interaction with the JBD. In this case an unstructured grid consisting of 37×10^6 cells was used. In [5], the interaction of the nonisobaric supersonic jets with total temperatures of $T_0 = 300$ and 600 K with an JBD placed at a distance of $X_{JDB}/D_e = 15$ from the nozzle exit was studied by the RANS/ILES method [12]. The distribution of the pressure pulsations near the airdrome surface and near the JBD were obtained. The calculations were performed for a structured grid consisting of 2.8×10^6 cells. The calculation accuracy was estimated by comparing it with experimental results and with the results of calculations performed by the MILES method with a finer grid [9]. The noise in the far field for the same configuration and flow conditions as in [5] was studied in [13]. The safety zone was also determined according to pressure pulsations (the zone with pulsations no less than 140 dB). The calculations were performed for a grid consisting of 8.5×10^6 cells.

In the mentioned works, the studies were performed under laboratory conditions. The impact of the external flow (in particular, of the wind) and the ship's velocity impact (for the ship's deck aviation) were not considered. However, even a low-velocity coflow can influence the flow, expansion ratio, and turbulent pulsations in the jet and its vicinities and, as a result, the size of safety zone determined according to different parameters of the jets exhaust from the turbojet engines. A study [14] verifies this fact. This work showed, with calculations performed by the RANS methods, that the wind greatly influences the jet flow near the JBD under the aircraft during liftoff from the ship's deck.

The goal of the present work is to study by the RANS/ILES method [12] the influence of the distance from the nozzle exit to the JBD and the coflow wind velocity on the turbulence parameters in the vicinity of a hot, nonisobaric, supersonic jet with a total temperature at nozzle input of $T_0 = 1050$ K and $\pi_c = 4$. The influence of the mentioned parameters on the size of the safety zone as determined by the temperature, pressure, and velocity pulsations near the airdrome surface and the temperature and pressure distribution and their pulsations at the JBD is determined.

COMPUTATION METHOD AND BOUNDARY CONDITIONS

The combined RANS/ILES method with high resolution described in [12] was used for calculations. In the Navier–Stokes equations, the convective fluxes at the cell faces were calculated by the Roe method. The required parameters were determined by a low-diffusion monotonous scheme of the ninth order with upwind finite-difference scheme [15]. The monotonous scheme makes it possible to calculate the supersonic flow with shock waves. The convective fluxes at cell faces in difference analogs of passive admixture transport equations (for the model of turbulence, passive admixture transport and etc.) were calculated with the scalar analog of Roe method, and the pre-decay parameters at cell faces were calculated with the WENO5 scheme [15]. The diffusion flows in the Navier-Stokes equations and in the transport equations were determined for cell faces with central-difference approximations of the second order.

Near walls, the flow is described by the unsteady RANS method with the Spalart–Allmaras turbulence model [16]; far from the walls, the flow is described by the LES method. In the described method there is no explicit SGS model of turbulence. The scheme viscosity (LES with implicit SGS-model—ILES) plays its role. In ILES zone turbulent viscosity should be equal to zero. It was obtained by modifying the distance in the dissipative term in the equation for turbulence model [16]. The new distance $\tilde{d}$ was calculated as follows [12]:

$$\tilde{d} = d \text{ with } d \le C_{ILES}\Delta_{max},$$

$$\tilde{d} = 0 \text{ with } d > C_{ILES}\Delta_{max}.$$

Here, d is the true distance from the wall to the center of the examined cell; $C_{ILES} = 0.65$ is a parameter that determines the place at which RANS is replaced by ILES; and Δ_{max} is the maximal size of grid cell.

Other details of the numerical method are presented in [12]. The described method was successfully used to calculate complicated subsonic and supersonic jet flows [5, 12, 13] and for unsteady supersonic flows with a complicated sock-wave structure in supersonic diffusers [18].

The boundary conditions for calculations for the jet without coflow are presented in [12]. It is not very simple to formulate boundary conditions at the exter-

nal boundary of the computational domain in the problem of near-wall jet interaction with the JBD. This is true, because, for a certain part of the boundary, the flow enters the computational domain (as it does for the free jet) and, for another part near the JBD, it exits the computational domain. We do not know in advance where the line separating these areas is. The combined boundary condition presented in [13] is used. For this part of the boundary, where the velocity in the center of the cell nearest to the boundary is directed outside, conditions corresponding to the output boundary of the computational domain are set. For the other part of the external boundary of the computational domain, the far-field condition for the jet without coflow is used [12]. If there is coflow at the external boundary of computational domain, the total parameters of the flow and the angle of inclination for velocity vector are set. The combined boundary condition "wall function"/no-slip are set on the walls. The conditions are chosen according to the boundary-layer coordinate Y^+ in the center of cell nearest to the wall.

CALCULATION ACCELERATION

If the turbulent flow is simulated numerically by vortex-resolved approaches using grids with a high number of cells, the problem of efficient calculations resolving flow features within a small period of time becomes important. This problem is solved by code parallelization with procedures that make it possible to perform efficient calculations with supercomputers with a given architecture. Below, we present parallelization features intrinsic to the RANS/ILES method.

The computation procedure [12] is implemented in the form of code written in the Fortran 95 environment. The calculations were performed in Joint Supercomputer Center of the Russian Academy of Sciences with a MVS-10P supercomputer with parallelization features intrinsic to this computer. The code is optimized and implemented with an Intel Xeon E5-26908-core processor. Each MVS-10P computation node consists of the two mentioned processors. Code optimization within a processor is performed by computation vectorization to use AVX commands, and OpenMP technology is also used for cycle nest parallelization. The MPI technique is used to distribute computations over several supercomputers. The calculations are performed in block-structured grids. The total number of grid blocks should be sufficiently high: several blocks per one computation node. When the calculations are distributed over several computational nodes of supercomputer, each grid block is connected statically to the computational node at the beginning of program operation. After that, each computational node processes grid blocks related just to this node, and the neighbor blocks connected to different computational nodes are changed by the physical performances of their neighboring cells by the MPI technique.

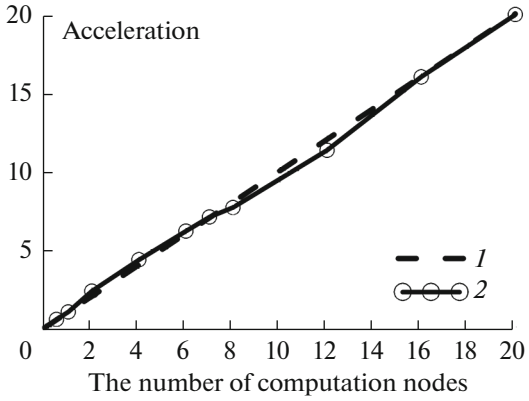

Fig. 1. Computation scalability for calculation nodes of the MVS-10P supercomputer: (*1*) linear acceleration, (*2*) real acceleration for computation code.

Balancing algorithms are used to distribute calculations uniformly over the supercomputer nodes. These algorithms make it possible to distribute grid blocks over different computational nodes. The test calculation on the interaction of the airdrome jet exhaust from the TJE with the JBD was performed on a grid consisting of 136 blocks containing 8.5×10^6 cells. The high number of grid blocks and their nearly optimal distribution over supercomputer computational nodes resulted in the practically linear scalability of distributed calculations up to 20 supercomputer nodes. Figure 1 depicts this process.

CALCULATION RESULTS

We studied how the nonisobaric, supersonic airdrome jet generated by TJE interacts with the JBD at $T_0 = 1050$ K and $\pi_c = 4$. These parameters were taken from [14, 18], and they are close to the real values. The jet flowed from a biconical nozzle with the following sizes: the diameter of subsonic part is 79.35 mm, the diameter of the critical cross section was 67.06 mm, and the diameter of the output cross section was 72.85 mm. The length of subsonic part was 9.8 mm, and the length of the supersonic part was 73.56 mm. A cylindrical segment with length of 80 mm was connected to the nozzle on the left for the convenient setting of boundary conditions. The Reynolds number was calculated according to the velocity in the output cross section of the nozzle and, according to its diameter D_e, was equal to 8.8×10^5. The wind velocity U_w (of the coflow) varied in calculations. In the first case, $U_w = 0$. After that we simulated aircraft liftoff from the ship's deck with a velocity of 24 knots [14], which corresponds to $U_w = 12$ m/s. We also studied the case in which the ship moves upwind, blowing at 8 m/s. In this case the total $U_w = 12$ m/s. It corresponds to the conditions in which the aircraft stands at the airdrome near the JBD and the coflow wind blows with veloci-

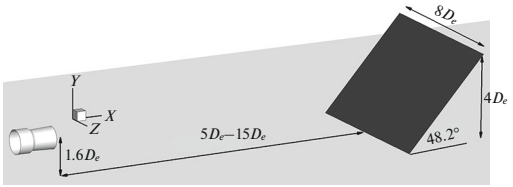

Fig. 2. Block diagram of nozzle and JBD disposition.

ties of 12 and 20 m/s, which corresponds to the Mach numbers of 0.035 and 0.059. We disregarded the thickness of the boundary layer on the airdrome or ship's deck surface. To increase the accuracy of the flow description in the jet mixing layer near nozzle exit, we jointly calculated the flow in the biconical nozzle, the geometry of which is described in [18], and in the jet. Figure 2 depicts the nozzle and JBD dispositions. Calculations were performed for two distances from the nozzle exit to the JBD: $X_{\text{JBD}}/D_e = 5$ and 15 for grids 6.33×10^6 and 8.53×10^6 cells, respectively.

We first present the results describing the influence of U_w and the JBD position X_{JBD} on the jet flow and the sizes of the area in which temperature values are higher than 350 K. Figure 3 depicts the fields of instantaneous and averaged longitudinal velocities in the longitudinal section $Z = 0$ crossing the nozzle axis for an jet without coflow and at $U_w = 20$ m/s for an JBD position at $X_{\text{JBD}}/D_e = 15$.

The wind decreases the thickness of the mixing layer; as a result, the velocity at the jet axis decreases more slowly, and the supersonic segment of the jet lengthens (Figs. 3b and 3d). In addition, the wind deflects the jet above the JBD. At the jet's periphery, the wind impact is the most pronounced: it changes the shape, boundary, and sizes of safety zone for temperature. This can be seen from Fig. 4, in which isolines $T \geq 350$ K and the streamlines projections near airdrome surface are presented for different U_w. We see strong transversal jet spreading over the airdrome surface before the JBD: at $U_w = 0$, it reaches $24D_e$. The right boundary of safety zone is at $X/D_e = 16$–17. If the wind velocity increases, the lateral wings turn towards the positive direction of axis X, and their width decreases a bit. In the cross sections (depending on conditions), their thickness is $(0.3$–$0.7)D_e$. If U_w increases, the width of safety zone decreases and its right boundary shifts downstream.

If the jet interacts with an JBD placed at a distance of $X_{\text{JBD}}/D_e = 5$, the wind velocity practically does not influence the flow structure inside the jet. The correlation between U_w and the shape of safety zone for temperature is the same as it is for $X_{JBD}/D_e = 15$.

Analysis of the results showed that the proximity of the JBD to the nozzle and the presence of wind more strongly influence the nature of the flow near the airdrome surface than for variants with $X_{\text{JBD}}/D_e = 15$. This is seen in Fig. 5, which shows the isolines of static temperature $T \geq 350$ K and the streamlines projections at a small distance from airdrome surface. It is seen that, at $U_w = 0$, a reverse flow spreads out like a fan. This leads to a strong transversal jet flow. In this case the width of safety zone for temperature is about $27D_e$. If the wind velocity increases, the area of reverse flow in the longitudinal direction decreases. For $U_w = 12$ m/s, it is approximately at $X = 0$, and it is at $X/D_e = 1$–3 for $U_w = 20$ m/s (depending on the transversal distance from jet axis). For all cases, the great transversal jet spreading is due to this reverse flow.

The coflow greatly influences the temperature pulsation distribution over the airdrome surface. For an JBD at $X_{\text{JBD}}/D_e = 15$, we see that, if the wind velocity increases, the area with a relatively high level of temperature pulsation $T' \geq 20$–25 K becomes more compact in the transversal direction ($13D_e$ at $U_w = 0$ and $10D_e$ at $U_w = 20$ м/с). Also it does not turn downstream. In all cases a pulsation maximum of 50–55 K is seen at distances of $(1$–$1.5)D_e$ upstream from JBD ends. In addition, if there is wind, an area with increased temperature pulsations that we do not see for the jet without coflow appears behind the JBD.

The reverse flow near the surface for variants with $X_{\text{JBD}}/D_e = 5$ widens the area with increased pulsations with respect to the JBD at $X_{\text{JBD}}/D_e = 15$. Their peak values become higher by 1.5 times with respect to the JBD at $X_{\text{JBD}}/D_e = 15$. In addition, if the wind velocity increases, the peak values of temperature pulsations rises from 55 K at $U_w = 0$ up to 70 K at $U_w = 20$ m/s. If there is no coflow, the viscous pulsations are localized

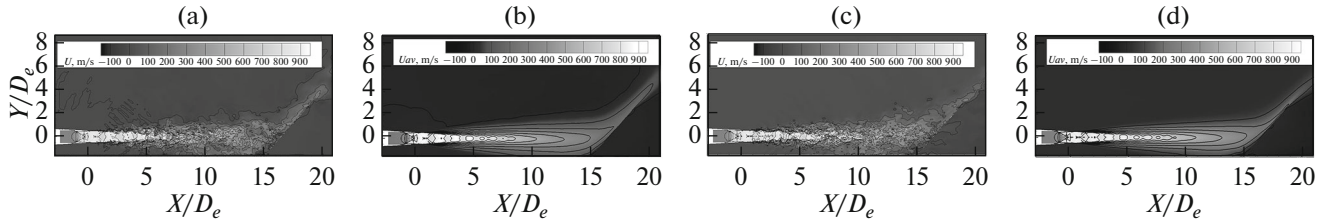

Fig. 3. Fields of instantaneous (a), (c) and averaged (b), (d) longitudinal velocities at hot, near-wall jet interaction with the JBD at $X_{\text{JBD}}/D_e = 15$: (a), (b) $U_w = 0$; (c), (d) $U_w = 20$ m/s.

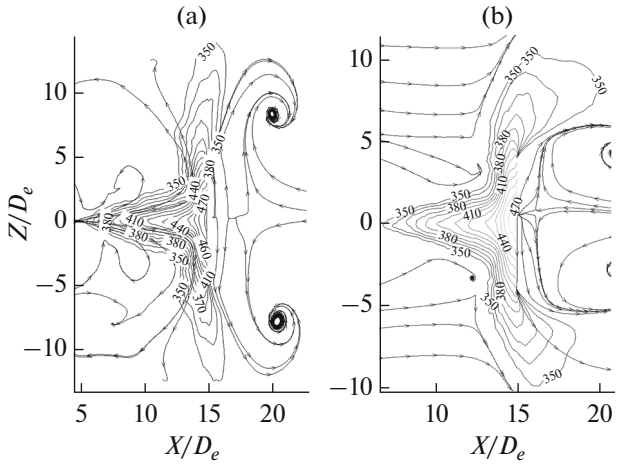

Fig. 4. Influence of wind velocity on the size and shape of the safety zone for a temperature of $T \geq 350$ K and on the flow near the Earth's surface for variants with $X_{JBD}/D_e = 15$: (a) $U_w = 0$, (b) $U_w = 20$ m/s.

only near the JBD, where the jet decelerates. The peak values occur at a distance of $(2–3)D_e$ from the jet axis, not near the JBD edges. Due to jet spreading caused by reverse flows, the velocity in the jet rises rapidly, and the pulsation level in the other part of the jet near the airdrome surface is therefore not high.

The jet exhaust from the turbojet engine nozzle generates high-power pressure pulsations, which can be dangerous for people, machinery, and equipment. This is why it is necessary to know the pressure pulsation on the airdrome surface and on the JBD and the sizes of the area where they reach dangerous values, as well as the influence of wind velocity on these parameters. Figure 6 depicts the influence of wind velocity on the shape and size of the area on the airdrome surface in which the level of pressure pulsations is higher than 140 dB. It is seen that, if U_w increases, the maximal width of this area decreases. In addition, if U_w increases after the JBD, the pressure pulsation level rises. It is necessary to point out that the left boundary of the safety zone is placed at the distance of $(1–3)D_e$ upstream from nozzle exit. Its width at $X = 0$ is $(14–15)D_e$, and it is practically independent of wind velocity. At a distance of $X/D_e = 2–5$ on the airdrome surface, we see the area with a high pulsation level: approximately 170 dB. Here, the turbulent mixing layer touches the airdrome surface (Fig. 5). It is interesting that the area with a high pulsation level of 140–148 dB widens downstream, after the JBD, and the position of its left boundary depends insufficiently on U_w. If the wind velocity increases, the shape of safety zone after the JBD becomes close to a triangle (Fig. 6), and it changes insufficiently if U_w increases from 12 up to 20 m/s.

At $X_{JBD}/D_e = 5$, the relationship between the shape and size of the safety zones and pressure pulsations changes a bit. Figure 7 shows their dependence on U_w. It is necessary to point out that the shape of the area with a high pulsation level differs from the shape observed for the JBD at $X_{JBD}/D_e = 15$, and the maximal width of safety zone for the JBD at $X/D_e = 5$ is lower. However, at small distances from the nozzle exit, the width of the safety zone for the JBD at $X_{JBD}/D_e = 5$ is approximately $20D_e$ at $U_w \leq 12$ m/s; for the variant with $X_{JBD}/D_e = 15$ it is equal to $16D_e$. It is necessary to point out that, for both JBD positions, we see an area with a pressure pulsation level not lower than 168 dB. It starts at $X/D_e = 3$: here, the turbulent mixing layer touches the airdrome surface. The maximal pressure pulsation level is observed near the JBD bottom. It is practically independent of X_{JBD} and U_w, and it is equal to 172–174 dB.

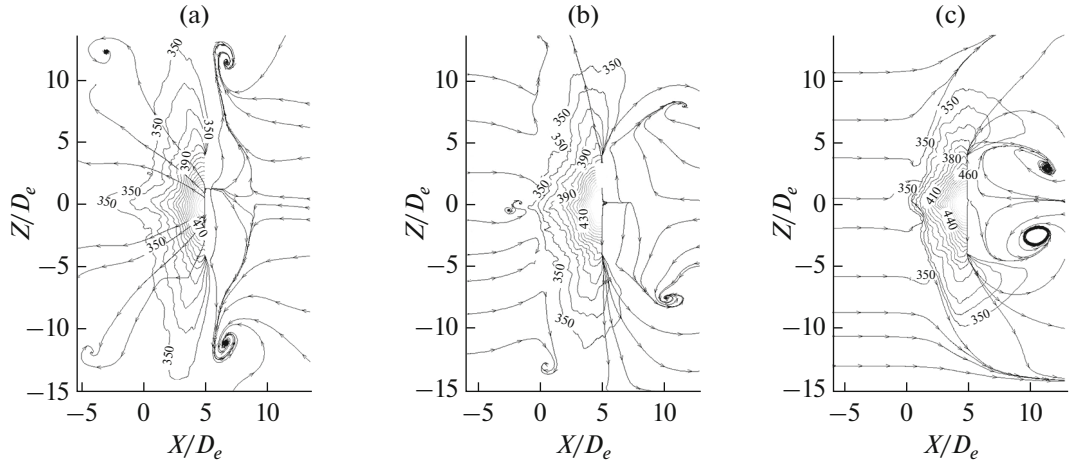

Fig. 5. Influence of wind velocity on the size and shape of the temperature safety zone and the flow near the airdrome surface for variants with $X_{JBD}/D_e = 5$: (a) $U_w = 0$, (b) 12 m/s, (c) 20 m/s.

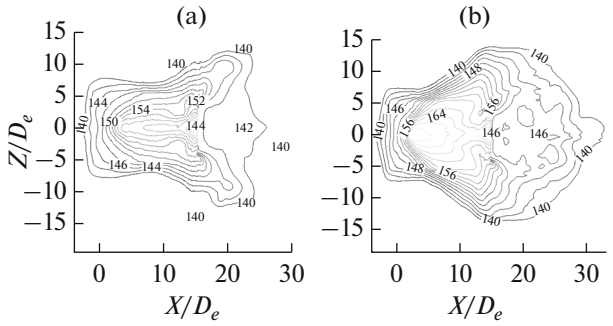

Fig. 6. Fields of static pressure pulsations and sizes of the safety zone at the airdrome surface for variant with $X_{JBD}/D_e = 15$: (a) $U_w = 0$, (b) 12 m/s.

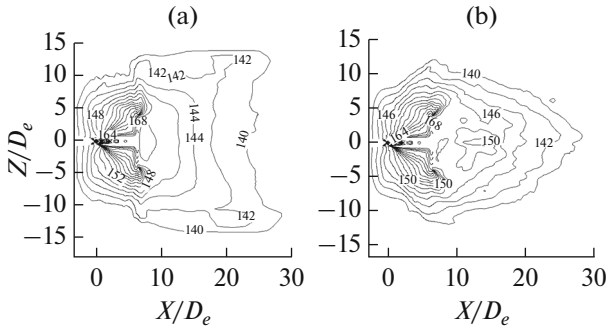

Fig. 7. Fields of static pressure pulsations at the airdrome surface for variant with $X_{JBD}/D_e = 5$: (a) $U_w = 0$, (b) 20 m/s.

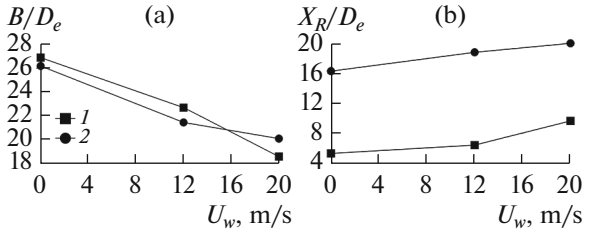

Fig. 8. Influence of the distance to the JBD and wind velocity on the width (a) and position (b) of the right boundary of the temperature safety zone: (*1*) $X_{JBD}/D_e = 5$, (*2*) 15.

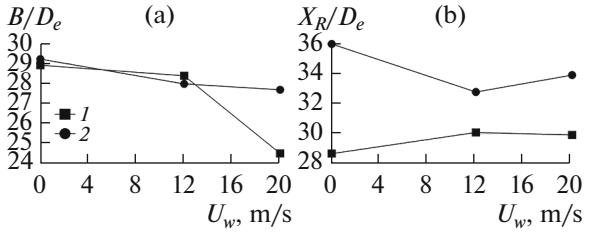

Fig. 9. Influence of the distance to the JBD and wind velocity on the width (a) and position (b) of the right boundary of the safety zone for pulsation pressure: (*1*) $X_{JBD}/D_e = 5$, (*2*) 15.

Based on the computation results, we determined the dependence of the size of the safety zones on the JBD position and wind velocity. Figure 8 depicts these relationships for the safety zone for temperature. Figure 9 depicts these relationships for the safety zone for pressure pulsations. It is seen that the wind velocity U_w most strongly influences the size of safety zone for temperature: if U_w rises to 20 m/s, its width decreases nearly by 1.5 times. The distance from the nozzle to the JBD weakly influences the width of this area. The dependence of the right boundary of this safety zone on U_w is also more pronounced for the temperature safety zone: if U_w rises to 20 m/s, the right boundary shifts by 20–25% downstream from the nozzle exit.

The width of the safety zone for the pressure pulsation level depends on U_w much more weakly, and this dependence decreases still more if the JBD moves off the nozzle. This is seen from 9a. The position of the right boundary of the safety zone for pressure pulsations changes insignificantly if the wind velocity changes (Fig. 9b). However, for the temperature and pressure pulsations, the position of the right boundary of safety zone depends greatly on X_{JBD}. It is necessary to point out that the right boundary of the temperature safety zone as a function of wind velocity and JBD position is determined at $X/D_e = 5$–20; for the safety zone for pressure pulsations, this boundary is at $X/D_e = 29$–36.

One more important characteristic of the near-wall jets is the safety zone for flow velocity near the airdrome surface. A velocity of $U \geq 15$ m/s is usually dangerous [1]. However, in our study, the wind velocity can be 20 m/s, and that is why we choose the more rigid condition. We determined the area for which $U \geq 30$ m/s. We analyzed this safety zone for velocity in the plane $Y = 0$ ($1.6D_e$ from the airdrome surface), where the sizes of this area are close to maximal, and we found that its greatest width is in the JBD cross section and downstream. At $U_w = 0$ the width of safety zone is about $10D_e$, and its right boundary is in the JBD cross section. For $U_w = 12$ m/s the maximal width is $23D_e$, and the right boundary is at $X/D_e = 30$. At $U_w = 20$ m/s the maximal width and position of right boundary are the same. If the JBD moves off the nozzle exit, the length of the safety zone increases at the same U_w. This is seen from Fig. 10.

It is necessary to point out that, below the JBD in the presence of wind, an area with high velocities is described by two "wings," as it is for the temperature distribution, but they are more curved and elongated. Their maximal width is $(4–5)D_e$ (Fig. 10b).

In practice it is necessary to know the distributions for pressure, temperature, and their pulsations at the JBD. We analyzed the calculation results and found that the jet mostly influences an JBD placed at a distance of $X_{JBD}/D_e = 5$. Figure 11 depicts the pressure and temperature distributions over an JBD height in

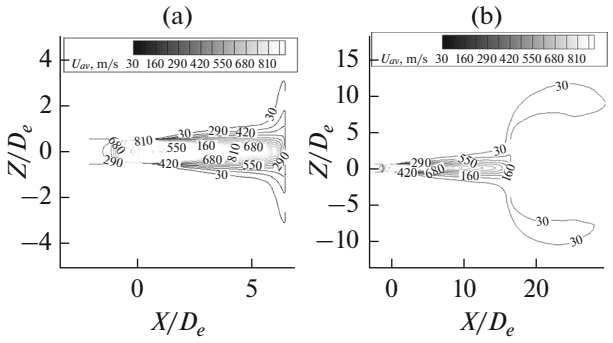

Fig. 10. The influence of the JBD position at $U_w = 12$ m/s on the size of the safety zone $U \geq 30$ m/s in the cross section $Y = 0$: (a) $X_{JBD}/D_e = 5$, (b) 15.

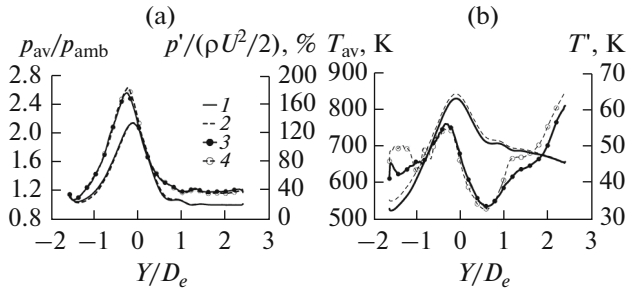

Fig. 11. Influence of wind velocity U_w on the distributions over the JBD height at $X_{JBD}/D_e = 5$ in cross section $Z = 0$: (a) pressure and static pressure pulsations, (b) temperature and its pulsations; (*1*) p_{av} (T_{av}), $U_w = 0$; (*2*) p_{av} (T_{av}), $U_w = 20$ m/s; (*3*) p' (T'), $U_w = 0$; (*4*) p' (T'), $U_w = 20$ m/s.

the section $Z = 0$ crossing the jet axis. The peak pressure value at the JBD is 2.15 times higher than the ambient pressure p_{amb}, and the peak temperature value is about 825 K. The vertical coordinate at which the maximum values of these parameters is observed is somewhat lower than the nozzle axis and is equal to $Y/D_e = -0.1$. This is due to jet interaction with the airdrome surface: the jet warps, and its axis shifts downward [5]. From Fig. 11, it is seen that the distributions of pressure and temperature pulsations over the JBD height is practically independent of U_w. The pressure and temperature maximums are at the jet axis and, as was mentioned above, the coflow does not influence the jet core at such small distances. The peak values of pressure pulsations (Fig. 11a) are of 180% of the velocity pressure at the nozzle exit. Such a high pressure pulsation level is due to the fact that the jet is not isobaric and the velocity at the jet axis is high in the JBD cross section. Temperature pulsation at the same JBD height is about 55 K. It is necessary to point out that the maximum of temperature pulsations at this JBD position takes place at its upper edge and is equal to 60–63 K (Fig. 11b).

The impact of a jet is much weaker on an JBD at $X_{JBD}/D_e = 15$: at this distance, the velocity and turbulence parameters in the jet are lower than at $X_{JBD}/D_e = 5$. The maximal pressure rise is 22% from p_{amb} at $U_w = 0$ and is 25% at $U_w = 20$ m/s. The peak static pressure increases if U_w increases, since the coflow decreases the jet spread and the velocity at the jet axis is high in the cross section of the JBD. The pressure maximum is lower than the nozzle axis, and this shift is $(0.3–0.4)D_e$. The static temperature distribution has no pronounced maximum; it is practically constant over the JBD height and corresponds to a jet's total temperature in this cross section of 530 K. The relationship between pressure pulsations and T_0 and U_w is qualitatively the same as it is for static pressure. At wind velocities of $U_w = 12–20$ m/s, the p' level is 20% higher than for the jet without coflow and it is 40% of the dynamic pressure at the nozzle exit. The level of temperature T' pulsations increases if U_w increases. Maximal T' is seen at $U_w = 20$ m/s and it is 32 K.

CONCLUSIONS

We numerically studied the influence of the wind velocity U_w (0, 12 and 20 m/s) and the distance from nozzle exit X_{JBD} ($X_{JBD}/D_e = 5$ and 15) on the flow in the vicinity of a nonisobaric, supersonic, hot airdrome jet at $T_0 = 1050$ K and $\pi_c = 4$ inflow to the JBD. The sizes of the safety zones for temperature, pressure, and velocity pulsations are determined near the airdrome surface. They were calculated by the combined RANS/ILES method with structured grids consisting of 6.33×10^6 and 8.53×10^6 cells.

If the JBD is placed at $X_{JBD}/D_e = 15$, the wind velocity greatly influences the size and shape of the safety zone for a temperature of $T \geq 350$ K. If U_w increases from 0 to 20 m/s, the width of safety zone decreases from $26D_e$ to $20D_e$ and its right boundary shifts from $X/D_e = 16$ to $X/D_e = 20$. The width of the safety zone at the airdrome surface with a pressure pulsation higher than 140 dB decreases from $29D_e$ to $28D_e$ if U_w increases to 20 m/s. In this case its left boundary is placed at a distance of $(1–3)D_e$ upstream relative to the nozzle output cross section, and the right boundary shifts from $X/D_e = 36$ to $X/D_e = 34$.

If the JBD is placed at $X_{JBD}/D_e = 5$, the jet spreads transversally near the airdrome surface, practically just at nozzle exit. The coflow greatly influences flow behavior near the airdrome surface. At $U_w = 0$ near the surface, reverse flows spread out like a fan. This causes strong jet spreading; the width of temperature safety zone is about $27D_e$. If U_w increases, the reverse flow area in longitudinal direction decreases: for $U_w = 20$ m/s, the width of the safety zone decreases down to $19D_e$. The width of the area with a pressure pulsation level higher than 140 dB U_w is the same as it is if the JBD is at $X_{JBD}/D_e = 15$. If U_w increases to 20 m/s, the width decreases to $25D_e$.

We analyzed the size of the area with a velocity level of $U \geq 30$ m/s in plane $Y = 0$ and found that, if the JBD moves off the nozzle exit for fixed U_w, its length increases. At $U_w = 0$, its width is about $10D_e$, and the right boundary is in the JBD cross section. For U_w = 12–20 m/s, the maximal width is $23D_e$, and the right boundary is placed at $X/D_e = 30$. In this case downstream relative to the JBD, the safety zone has the shape of two "wings". Their maximal width is about of $(4–5)D_e$.

The maximal sizes for both JBD positions has a safety zone for pressure pulsations. Its width is $(30–24)D_e$, and the right boundary is at $(26–35)D_e$ for U_w= 0–20 m/s.

We analyzed the flow parameter distribution over the JBD height and found that, for variant with $X_{JBD}/D_e = 15$, the peak pressure value increases if U_w increases. The temperature distribution has no pronounced maximum. The relationship between pressure pulsations and U_w is qualitatively the same as it is for the pressure. If U_w increases to 20 m/s, the level of pressure pulsations rises by 20% with respect to its level at $U_w = 0$. The temperature pulsations increase if U_w rises. Maximal T' takes place at $U_w = 20$ m/s; it is 32 K.

For an JBD at $X_{JBD}/D_e = 5$, there is no correlation between U_w and the pressure and temperature distributions and the distributions of their pulsations over the JBD height. The peak pressure value at the JBD is 2.15 times higher than the ambient pressure, and the peak temperature value is about 825 K. The maximal values of pressure pulsations are 10% of the velocity pressure at the nozzle exit. The maximum temperature pulsation is 60–63 K.

ACKNOWLEDGMENTS

This work is supported by the Russian Foundation for Basic Research, project no. 15-08-01996A.

REFERENCES

1. Khritov, K.M., Lyubimov, D.A., Maslov, V.P., Mineev, B.I., Secundov, A.N., and Birch, S.F., Three-dimensional wall jets: Experiment, theory and application, *AIAA Pap.* 2002-0732, 2002.
2. Agelin-Chaab, M. and Tachie, M.F., *Int. J. Heat Fluid Flow*, 2011, vol. 32, p. 608.
3. Davis, M.R. and Winarto, H., *J. Fluid Mech.*, 1980, vol. 101, p. 201.
4. Ishiko, K., Hasimoto, A., Matsuo, Y., Yoshizawa, A., Nishiyama, Y., and Nakamura, Y., *J. Aircr.*, 2014, vol. 51, no. 2, p. 584.
5. Benderskii, L.A., Lyubimov, D.A., Potekhina, I.V., and Fedorenko, A.E., *Uch. Zap. TsAGI*, 2016, vol. 47, no. 2, p. 36.
6. Berch, S.F., Lebedev, A.B., Lyubimov, D.A., and Sekundov, A.N., *Fluid Dyn. (Engl. Transl.)*, 2001, vol. 36, no. 5, p. 712.
7. Lyubimov, D.A., *Aeromekh. Gaz. Din.*, 2003, no. 3, p. 14.
8. Worden, T.J., Gustavsson, J.P.R., Shih, C., and Alvi, F.A., Acoustic measurements of high-temperature supersonic impinging jets in multiple configurations, *AIAA Pap.* 2013-2187, 2013.
9. Liu, J., Corrigan, A., Kailasanath, K., Ramammurti, R., Heeb, N., Munday, D., and Gutmark, E., Impact of deck and jet blast deflector on the flow and acoustic properties of imperfectly expanded supersonic jets, *AIAA Pap.* 2013-323, 2013.
10. Erwin, J.P., Sinha, N., and Rodebaugh, G.P., Noise predictions of a hot twin-jet impinging on a jet blast deflector, *AIAA Pap.* 2013-324, 2013.
11. Khalighi, Y., Nicholsy, J.W., Lele, S.K., Ham, F., and Moin, P., Unstructured large eddy simulation for prediction of noise issued from turbulent jets in various configurations, *AIAA Pap.* 2011-2886, 2011.
12. Lyubimov, D.A., *High Temp.*, 2012, vol. 50, no. 3, p. 420.
13. Benderskii, L.A. and Lyubimov, D.A., Abstracts of Papers, *IV Otkrytoi vseros. konf. po aeroakustike* (IV Open All-Russia Conf. on Aeroacoustics), Moscow, 2015, p. 112.
14. Kuizhi, Y., Liangliang, C., Hu, L., and Yunliang, W., *Aerosp. Sci. Technol.*, 2015, vol. 45, p. 60.
15. Suresh, A. and Huynh, H.T., *J. Comput. Phys.*, 1997, vol. 136, no. 1, p. 83.
16. Spalart, P.R. and Allmaras, S.R., *Rech. Aerosp.*, 1994, no. 1, p. 5.
17. Lyubimov, D.A. and Potekhina, I.V., *High Temp.*, 2016, vol. 54, no. 5, p. 737.
18. Liu, J., Kailasanath, K., Munday, D., Nick, H., and Gutmark, E., Large-eddy simulations of a supersonic heated jet, *AIAA Pap.* 2011-2884, 2011.

Translated by Yu. Zikeeva